EasyChair Preprint

№ 1319

Improvement in measurement area of three-dimensional LiDAR using mirrors mounted on mobile robots

Kazuki Matsubara and Keiji Nagatani

July 21, 2019

Improvement in measurement area of three-dimensional LiDAR using mirrors mounted on mobile robots

Kazuki Matsubara, Keiji Nagatani

Abstract By installing omnidirectional measurement light detection and ranging (LiDAR) on a mobile robot, it is possible to acquire the surrounding environment. However, not all measurement areas of LiDAR can be used because of laser rays blocked by the robot's body. Hence, in this research, the authors aim to expand the measurement area of LiDAR by installing mirrors at the blocked area to improve an ability of acquiring information regarding the front environment. The installation position and mirror angle can be determined from the desired area to be measured and the geometrical condition of the laser rays reflecting on the mirror. Moreover, based on the method, the robot enabled to collection of the surface information of stairs during stair climbing, which was typically difficult to gather.

1 Introduction

In recent years, the demand for automation of plant inspection using robot technology has increased. Reducing labor and increasing safety are important reasons behind this demand. Particularly, companies having offshore platforms expect to realize mobile robots for an autonomous inspection, because the burden on workers and the cost of labor are high [9]. Tracked vehicles are attracting attention as an option to achieve such tasks. They exhibit good traversal ability on steps/stairs and high loading capacity in installing various sensors. When traveling autonomously, this type of mobile robot is required to generate an environmental map and/or to localize itself. Light detection and ranging (LiDAR) is often used to acquire infor-

Kazuki Matsubara
Tohoku University, 468-1, Aza-Aoba Aramaki, Aoba-ku, Sendai, Japan, e-mail: matsubara@frl.mech.tohoku.ac.jp

Keiji Nagatani
The University of Tokyo, 7-3-1 Hongo, Bunkyo-ku, Tokyo, 113-8656, JAPAN, e-mail: keiji@ieee.org

mation regarding the surrounding environment. Notably, an omnidirectional three-dimensional LiDAR (3D-LiDAR) that can acquire the 3D point cloud of the surrounding environment has become popular recently.

In general, omnidirectional 3D-LiDAR should be installed on the top of a mobile robot to measure omnidirectionally. However, when LiDAR is installed at the top of mobile robots, as shown in Figure 1(a), several problems arise. For example, the overall undetectable areas close to the robot increases, and the LiDAR may block other sensors' sensing area. The former issue is serious because of the risk of collision with obstacles or the increased possibility of the robot falling down from steps/stairs.

Hence, for expanding the measurable area, swinging the LiDAR itself [6] or installing multiple LiDARs are considered. However, mounting additional swinging functions or increasing the number of sensors is undesirable in terms of the weight and cost of the robot.

In-plant inspection robots, focused by the authors, rarely move backward. Therefore, an omnidirectional 3D-LiDAR is typically installed at the front of the mobile robot instead, as shown in Figure 1(b), to avoid the aforementioned problems. However, in this case, the robot body blocks the laser rays behind the sensor, and half of the sensor information that can be acquired originally is invalidated. Additionally, even in such a remaining available area, LiDAR still has a blind spot near the robot as its measurement range in the vertical direction is limited.

Therefore, in this research, to improve the environmental measurement area of LiDAR, the authors focus on the combination of LiDAR and mirrors. Installing mirrors behind LiDAR, as shown in Figure 1(c), enables the invalidated area behind the LiDAR to be utilized. Hence, it is possible to acquire environmental information within a broader range in front of the robot. Particularly, by expanding the measurement area to the lower front of the robot, it is possible to obtain terrain information such as a shape of the stairway or large obstacles in the short distance of the robot [4, 8, 10].

In the previous studies on the combination of LiDAR and mirrors, S.Abiko et al. proposed a method to expand the measurement area of LiDAR by combining a two-dimensional LiDAR and mirrors to enhance the environment recognition ability of flying robots [1]. Additionally, H.Noguchi et al. proposed a method to obtain a 3D point cloud with high density by combining a two-dimensional LiDAR with mirrors and a rotation mechanism [5]. However, studies that combine 3D-LiDAR and mirrors for inspection robots are non-existent, to the author's best knowledge.

Herein, the installation condition of the mirror is proposed to obtain information regarding the desired measurement area with invalidated laser rays. Subsequently, an experimental report is described to evaluate the validity and accuracy of the proposed method. Furthermore, short experiments with a tracked vehicle are reported to acquire the point cloud in a real environment.

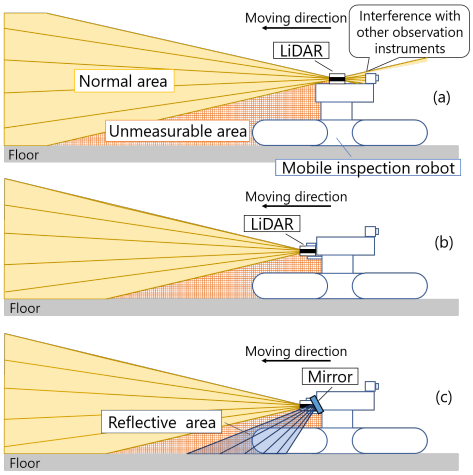

Fig. 1 Outline drawing of mobile inspection robot and explanation of measurable area of LiDAR: (a)LiDAR installed at the top of the robot, (b)LiDAR installed at the front of the robot, (c)LiDAR installed at the front of the robot with mirrors.

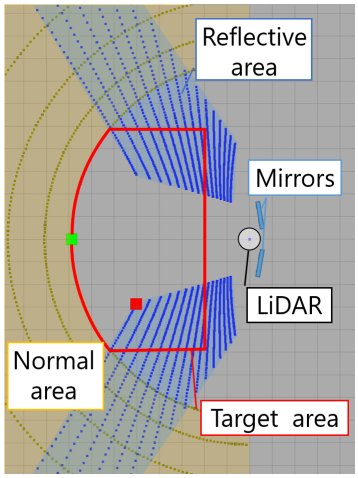

Fig. 2 How the laser spread after reflection

2 Installation condition of mirrors to acquire desired detection areas

2.1 Mirror installation requirements

To expand the measurable area of LiDAR by combining mirrors and omnidirectional 3D-LiDAR installed in front of the mobile robot, the following requirement should be satisfied:

- The overlap between the desired area to be observe (hereinafter called “target area”) and the detection area by the reflected laser ray (hereinafter called “reflective area”) is maximized.
- The overlap between the detection area of standard laser ray (hereinafter called ”normal area”) and the reflective area is minimized.

Moreover, in this research, the objective is to recognize obstacles at a short distance from the robot or the floor surface condition by expanding the measurable area. Therefore, the gap between the normal area and reflective area should be minimized.

Furthermore, two additional points in determining the installation angle of the mirrors are noteworthy.

- To use flat mirrors to avoid unintended laser ray behaviors due to the distortion of the mirrors’ surface or reflection of the laser light.

- To not locate the mirror at a position where the laser reflected by the mirror directly enters LiDAR to avoid LiDAR damage.

Based on the requirements above, the mirror installation angle is determined by solving the geometrical conditions shown in the next section. Note that, mirrors should be installed on the same base with LiDAR to avoid displacement of their surface caused by vehicle vibration during driving.

2.2 Geometrical conditions to satisfy requirements

Figure 2 shows an example of a geometric calculation result of the point cloud acquired using the normal laser ray and the laser ray reflected from mirrors, as shown in Figure 1(c). The yellow area corresponds to the normal area, the blue area corresponds to the reflective area, and the area surrounded by the red frame is the target area. The normal area extends concentrically around the LiDAR. Meanwhile, the reflective area is a quadrilateral where the point density decreases with distance from the center.

As shown in Figure 3, let the pitch angle α be the irradiation angle in the pitch direction of the laser ray, and let the yaw angle β be the irradiation angle in the yaw direction. The green point in Figure 2 shows the contact point between the laser ray and the floor, where α is the smallest and β is 0° among the normal laser rays. Further, the red point (hereinafter, a laser beam capable of acquiring this point called "target laser") represents a contact point between the laser ray and the floor, where α and β are the two largest among the reflected laser rays. Therefore, when the green point position corresponds with the red point position in Figure 2, the overlap area between the reflective area and target area is maximized, and the overlap area between the normal area and reflective area is minimized. However, the target laser has to be parallel to the xz plane to satisfy the prerequisite that the reflected laser should not enter the LiDAR directly. Based on the above,, to obtain the installation angle of a mirror that satisfies the requirements and the emphasize points in Section 2.1, the target laser should fulfill the following geometrical conditions:

1. The target laser satisfies the following conditions.
   - The irradiation angle in the pitch direction is the largest.
   - Laser ray reflected becomes parallel to the xz plane.
2. Let RV be the distance between the target laser and x-axis. This implies $y_r = RV$.
3. A plane representing a mirror passes through a point Q$= (x_q, y_q, z_q)$ with the following x, y, z coordinates:
   - x_q : x coordinate satisfying Y_q, θ_q shown in Figure 4 in the xy plane,
   - y_q : y coordinate with the value of Y_q shown in Figure 4
   - z_q : z coordinate satisfying $x = x_q, y = y_q$ on the laser ray with the largest irradiation angle in the pitch direction

Figure 3 shows the characters used under the geometric conditions above. Figure 4 shows the area where the mirror can be installed (hereinafter called "mountable area").

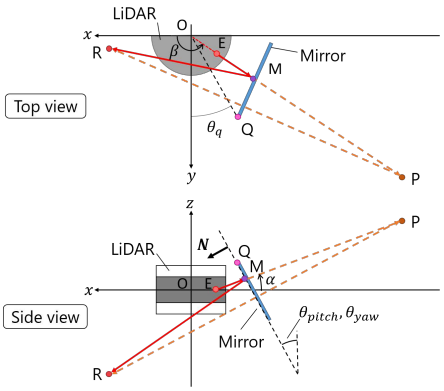

Fig. 3 Geometric conditions for determining mirror installation angle

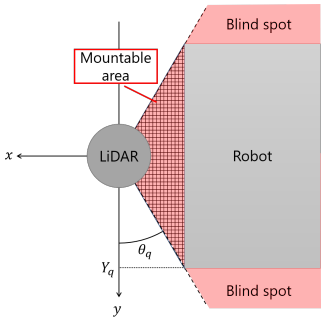

Fig. 4 Mountable area where mirrors can be installed

2.3 *Method of deriving mirror angle that satisfies design requirements*

In this section, the installation angle of the mirror is derived from the geometrical condition shown in Section 2.2. First, the irradiation angle β in the yaw direction from LiDAR is obtained such that the target laser is parallel to the xz plane after specular reflection. Let M be the point of intersection of the laser ray and the mirror surface, $\boldsymbol{N}$ be the normal vector of the mirror surface, and θ_{pitch} and θ_{yaw} be the rotation angles of the mirror's pitch direction and yaw direction, respectively. At this time, the normal vector $\boldsymbol{N}$ of the mirror surface can be described as Equation (1).

$$\boldsymbol{N} = \begin{pmatrix} \cos(\theta_{yaw})\cos(\theta_{pitch}) \\ \sin(\theta_{yaw})\cos(\theta_{pitch}) \\ -\sin(\theta_{pitch}) \end{pmatrix} = \begin{pmatrix} N_x \\ N_y \\ N_z \end{pmatrix} \tag{1}$$

To create a target laser ray that is parallel to the xz plane after specular reflection, the y coordinates of point M and point R should be RV. The irradiation angle β of the target laser beam in the yaw direction that satisfies this condition can be written as in Equation (2):

$$\beta = \sin^{-1}(\frac{X_1 - \sqrt{X_1^2 - X_2 X_0}}{X_2}). \tag{2}$$

It is noteworthy that X_0, X_1 and X_2 are expressed by Equation (4) using distance EP from the origin to the irradiation point of the laser ray and ξ represented by Equation (3).

$$\begin{aligned}\xi =& EP\cos(\alpha)N_z + \sin(\alpha)N_x x_q \\ &+ \cos(\alpha)N_y y_q + \cos(\alpha)N_z z_q - RV\sin(\alpha)N_y\end{aligned} \tag{3}$$

$$\begin{pmatrix} X_0 \\ X_1 \\ X_2 \end{pmatrix} = \begin{pmatrix} (RV\cos(\alpha)N_z)^2 - (RV\sin(\alpha)N_x)^2 \\ \xi RV\cos(\alpha)N_z \\ \xi^2 + (RV\sin(\alpha)N_x)^2 \end{pmatrix} \tag{4}$$

Next, obtain the mirror installation angles θ_{pitch} and θ_{yaw}. Let P be the coordinates obtained by the laser beam reflected by LiDAR, and E be the irradiation point of the laser beam. $\overrightarrow{EM}$ can be represented by the two equations (5) and (6) from Figure 3:

$$\begin{aligned}&\overrightarrow{EM} \\ &= \overrightarrow{EO} + \overrightarrow{OR} + \overrightarrow{RP} + \overrightarrow{PM} \\ &= (1 + \frac{L}{\boldsymbol{N}\cdot\overrightarrow{OR} - 2L - \boldsymbol{N}\cdot\overrightarrow{OE}})(\overrightarrow{OR} - 2L\boldsymbol{N} - \overrightarrow{OE}) \\ &= \boldsymbol{f}(\theta_{pitch}, \theta_{yaw}),\end{aligned} \tag{5}$$

$$\overrightarrow{EM} = \frac{\boldsymbol{N}\cdot\overrightarrow{EQ}}{\boldsymbol{N}\cdot\boldsymbol{n}}\boldsymbol{n} = \boldsymbol{g}(\theta_{pitch}, \theta_{yaw}). \tag{6}$$

It is noteworthy that L and $\boldsymbol{n}$ are the value represented by Equation (7) and the vector represented by Equation (8), respectively.

$$L = |(\overrightarrow{OR} - \overrightarrow{OQ})\cdot\boldsymbol{N}| \tag{7}$$

$$\boldsymbol{n} = \begin{pmatrix} \sin(\alpha)\cos(\beta) \\ \sin(\alpha)\sin(\beta) \\ \cos(\alpha) \end{pmatrix} \tag{8}$$

Here, both $\boldsymbol{f}(\theta_{pitch}, \theta_{yaw})$ and $\boldsymbol{g}(\theta_{pitch}, \theta_{yaw})$ represent the same $\overrightarrow{EM}$. However, depending on the values of θ_{pitch} and θ_{yaw}, $\boldsymbol{f}(\theta_{pitch}, \theta_{yaw})$ does not correspond with $\boldsymbol{g}(\theta_{pitch}, \theta_{yaw})$. $\boldsymbol{f}(\theta_{pitch}, \theta_{yaw})$ and $\boldsymbol{g}(\theta_{pitch}, \theta_{yaw})$ match only when θ_{pitch} and θ_{yaw} satisfy the geometrical conditions given in Section 2.2. Hence, the installation angle θ_{pitch} and θ_{yaw} of the mirror is a value that satisfies Equation (9).

$$\boldsymbol{f}(\theta_{pitch}, \theta_{yaw}) - \boldsymbol{g}(\theta_{pitch}, \theta_{yaw}) = \boldsymbol{0} \tag{9}$$

3 Verification test

According to the mirror installation requirements described in Section 2.2, a verification test was conducted to confirm the validity of the mirror installation requirements and the accuracy of the point cloud in the reflective area.

3.1 Test method

Figure 5 shows the test environment. First, the consistency between the reflective area and target area was verified by visualizing the point cloud that can be acquired from the laser ray reflected by the mirrors. Next, the target sphere with a height of 15 mm and a radius of 5 mm, covered by a highly reflective material, was placed in the target area, as shown in Figure 5. Subsequently, the measurement accuracy in the reflective area was verified by comparing the target sphere position obtained from the LiDAR and that from a manual. The target sphere was placed in 32 locations where the coordinates of the measurement target were $x = (300\,\mathrm{mm}, 500\,\mathrm{mm}, 700\,\mathrm{mm}, 900\,\mathrm{mm})$, $y = (|100\,\mathrm{mm}|, |200\,\mathrm{mm}|, |300\,\mathrm{mm}|, |400\,\mathrm{mm}|)$. In this test, VLP-16, manufactured by Velodyne, was equipped for LiDAR application. Its primary specification is shown in Table 1. From the LiDAR installation position and the mirror installation angle requirements described in Section 2.2, the size of $\boldsymbol{f}(\theta_{pitch}, \theta_{yaw}) - \boldsymbol{g}(\theta_{pitch}, \theta_{yaw})$ becomes that shown in Figure 7. As shown in Figure 7, the installation angle of the mirror was determined to be inward for 21.0° around the z-axis and 15.5° around the x-axis in Figure 3 because the size of $\boldsymbol{f}(\theta_{pitch}, \theta_{yaw}) - \boldsymbol{g}(\theta_{pitch}, \theta_{yaw})$ is the smallest. Figure 8 shows the reflective area calculated from the determined mirror installation requirements.

Table 1 Specification of Velodyne VLP-16

specification	Value
Number of lasers	16
detection area	(Horizontal) 360°, (Vertical) ±15°
measurement error	±3 cm (1 standard deviation at 25 m)
installation height	310 mm

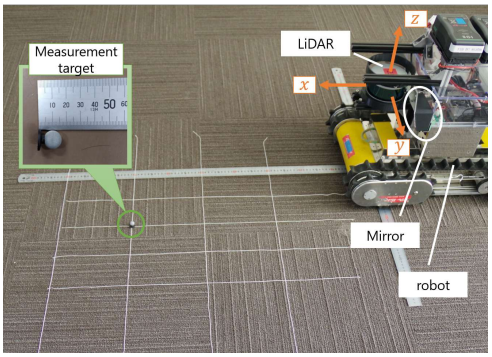

Fig. 5 Test environment

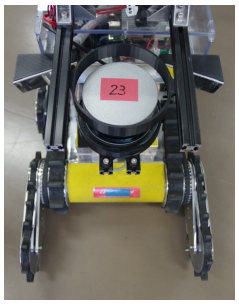

Fig. 6 Enlarged view of the mirror installation part

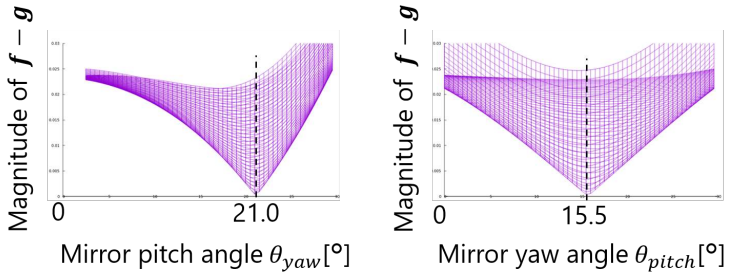

Fig. 7 Magnitude of $\boldsymbol{f}(\theta_{pitch}, \theta_{yaw}) - \boldsymbol{g}(\theta_{pitch}, \theta_{yaw})$ satisfying installation requirements

3.2 Calibration of Reflected Points

To reflect the point cloud obtained from LiDAR through the mirror surface, the normal vector information of the mirror surface and the position vector of the mirror is required. However, because of mirror installation errors, the coordinate transformation may be incorrect and the acquired point cloud in the reflective area will deviate from the actual values. Therefore, in this research, Rviz, a visualization tool for the robot operating system (ROS) [7] was used to correct the deviations of the normal vector of the mirror surface and the position vector. Figure 9 shows the appearance of Rviz while correcting the mounting angle of the mirror. The position and angle of the mirrors, shown as two plates in Rviz, can be changed manually by translating them along the x-axis and rotating them around the y- and z-axes. The calculation of coordinate transformation of the acquisition point cloud in the reflective area can be displayed in real time.

In this calibration step, the measurement target was placed at a position where both the normal laser and reflective laser can be measured. Subsequently, the correct position and angle of the mirrors were acquired by manually adjusting the mirrors,

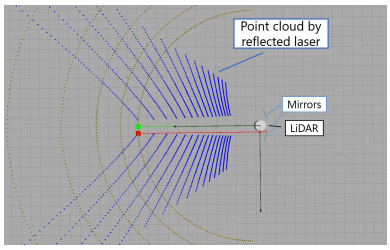

Fig. 8 Expected reflective area from calucu-lation

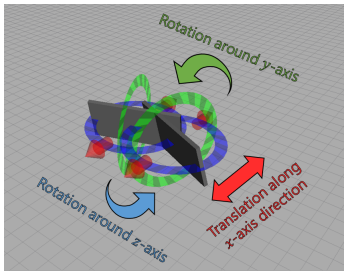

Fig. 9 Rviz appearance for mounting angle and position adjustment of the mirrors.

such that the measurement target obtained by the reflected laser ray corresponds with that obtained by the normal laser ray.

3.3 Results

Figure 10 shows the visualization of the resulting point cloud by Rviz. According to the comparison between Figure 8 and Figure 10, it was confirmed that the measurement area had expanded as designed. However, for the part surrounded by a green ellipse, the expected point cloud information could not be obtained.

Next, Figure 11 shows the position information of the detected target sphere projected onto the *xy* plane. Measurement and accuracy evaluation were performed at each intersection of the grid lines of the *x* and *y* axes, and the points indicate the average position of the acquired measurement target. The standard deviation of the error between the position information obtained by LiDAR and the measured value was 15 mm in the *xy* plane and 9 mm in the z direction.

3.4 Discussion

The point cloud that could not be acquired were all due to the laser ray with a large irradiation pitch angle α. Therefore, it is thought that the calculation results and the test results did not match owing to the installation error of the mirror.

Meanwhile, regarding the accuracy of the acquired point cloud, the errors in both the *xy* plane and *z*-axis direction are within the measurement error of LiDAR; therefore it can be concluded that the coordinate transformation is performed with sufficient accuracy.

In conclusion, the results indicate that the installation requirements of the mirror and the calculation results of the coordinate transformation are appropriate. Thus, environmental information can be acquired with sufficient accuracy from the point

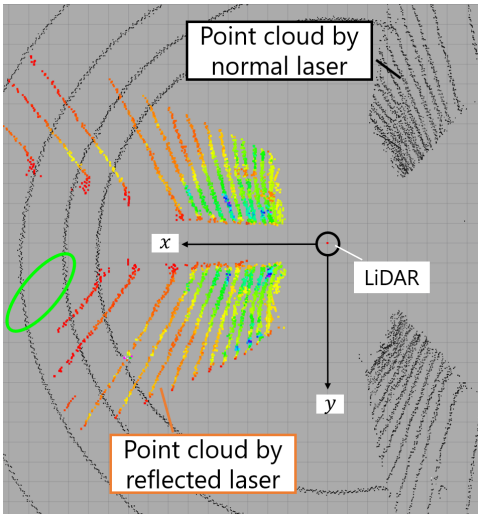

Fig. 10 Rviz visualization of resulting point cloud

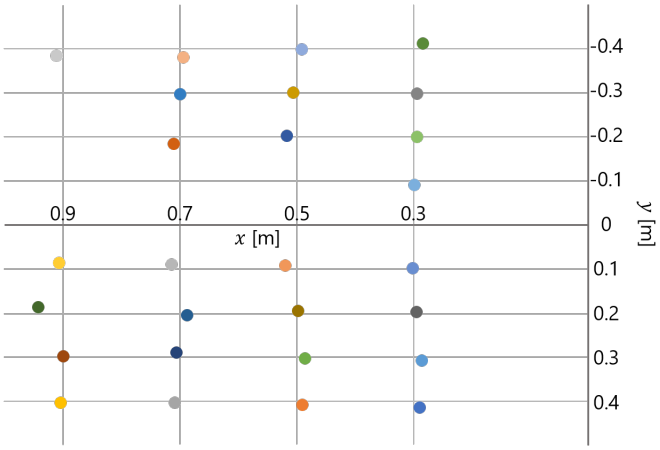

Fig. 11 Position information of detected measurement target projected onto xy plane

cloud in the reflective area by combining omnidirectional 3D-LiDAR and the mirror installed at the proposed installation angle.

4 Utility verification test in the proposed method

When a tracked vehicle inspects a plant, stairs are one of the places where movements becomes particularly hard. It is difficult to climb the stairs because in the case

of a standard LiDAR placement, environmental information cannot be obtained at short-range distances. In this section, we will report the effect of the tracked vehicle on stair climbing when using the proposed LiDAR measurement range expansion method.

4.1 Required information for a tracked vehicle to climb stairs

The environmental information related to the stairs, which is necessary for control when a tracked vehicle climbs stairs, includes the following for each scene[2, 3]:

- Start ascending: Slope of the starting step
- During ascend: Stairs' slope
- Finish ascending: Positional relationship between the landing step and the robot
- Start descending: Slope of the landing step
- During descend: Stairs' slope
- Finish descending: Height of the starting step, Stairs' slope

Among the scenes, the robot with the standard LiDAR installation cannot detect the stairs information of the following three scenes: during ascend, finish ascending, and start descending. Table 2 shows the information required for climbing stairs and current solutions for these scenes.

It is difficult to estimate a robot's status using odometry and inertial measurement unit (IMU) information owing to slips, disturbances, and gyroscope drifts [2]. In addition, although the installation of landmarks is considered as a practical solution, it is not always possible to install them and to not be acquired stably on any stairs. When it is not possible to acquire such stairs information, landing on the landing step may fail, and that may produce a strong impact to the robot, or in the worst case, the robot may fall downstairs. Therefore, by applying the proposed method combining LiDAR and mirrors to a robot, the robot can acquire the stairs information for climbing the stairs in all scenes.

Table 2 Necessary stairs information and current solutions when climbing stairs

Scene	Necessary stairs information	Current solutions
During ascend	Stairs slope	Measure the stairs' size in advance
Finish ascending	Positional relationship between the landing step and the robot	Place landmarks such as reflectors in the environment Measure the number of stairs in advance and measure the distance by odometry
Start descending	Slope of the landing step Positional relationship between the landing and the robot	Place landmarks such as reflectors in the environment Measure change in IMU information using sub crawlers

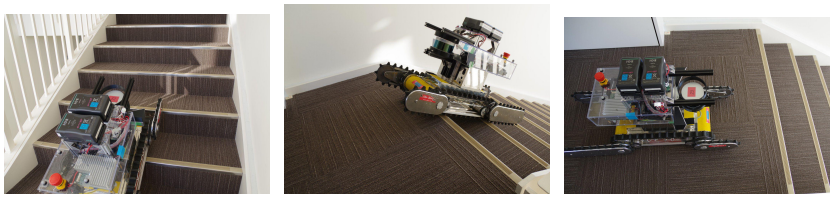

(a) During ascend (b) Finish ascending (c) Start descending

Fig. 12 Stairs environment and robot postures

4.2 Test method

To confirm whether the proposed method is effective for stair climbing by a tracked vehicle, an environment-recognition test was conducted for three real scenes: during ascend, finish ascending, and start descending, using real robots while traversing the stairs. Figure 12 shows the stairs environment in each scene. LiDAR and the position and angle of the mirrors are the same as in Section 3.

4.3 Test results

Figure 13 shows the recognition test results for the three scenes shown in Section 4.2.

As shown in Figure 13(a) for the ”during ascend” scene, it was possible to detect the cross section and edge of the stairs while ascending. According to the result, the robot can calculate the stairs' slope while climbing up the stairs. In addition, because the skirting board can be detected, the robot can estimate its position on the stairs.

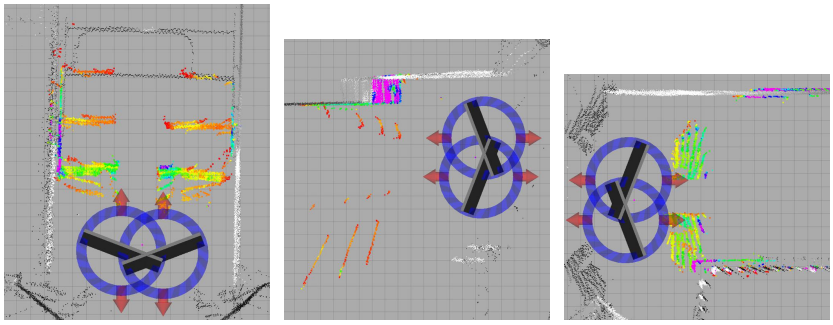

(a) During ascend (b) Finish ascending (c) Start descending

Fig. 13 Test results near stairs

As shown in Figure 13(b) for the ”finish ascending” scene at the end of the stairs, the surface of the landing step was acquired, although the sub-tracks blocked the reflective area detection. According to the result, it is possible to obtain the positional relationship between the landing step and the robot, which is crucial for a robot to land safely on the landing step of the stairs.

As shown in Figure 13(c) for the ”start descending” scene, the edge of the stairs near the downstairs was detected. In addition, because the skirting boards were detected, the robot can be positioned for ”start descending” without setting the landmarks in the environment. Based on the results above, it was confirmed that the robot acquired the necessary environment information for ascending/descending stairs by the additional two mirrors, which was difficult for the typical installation position of LiDAR.

Conclusion

In this research, the authors aim to expand the measurement area of LiDAR by additional mirrors behind omnidirectional 3D-LiDAR to improve an ability of acquiring information regarding the front environment. Hence, the design requirements of the mirror were proposed, the accuracy evaluation test of the detected point cloud was conducted, and the usefulness test in the real environment was performed. Although the reflective area was slightly different from the calculation results, it was confirmed that the position information of the obtained point cloud was acquired with practical accuracy.

In future works, based on the proposed method, the autonomy of tracked vehicles will be realized, such as obstacle detection and avoidance while traveling, and ascending/descending stairs with no environment information without any landmarks in advance.

Acknowledgements Mitsubishi Heavy Industries supported this work.

References

[1] Abiko S, Sakamoto Y, Hasegawa T, Yuta S, Shimaji N (2017) Development of constant altitude flight system using two dimensional laser range finder with mirrors. DOI 10.1109AIM.2017.8014121

[2] Endo D, Watanabe A, Nagatani K (2017) Stair Climbing Control for 4-DOF Tracked Vehicle Based on Internal Sensors. Journal of Robotics DOI 10.1109/SSRR.2016.7784286

[3] Guo J, Shi J, Zhu W, Wang J (2017) Approach to autonomous stair climbing for tracked robot. 2017 IEEE International Conference on Unmanned Systems (ICUS) pp 182–186, DOI 10.1109/ICUS.2017.8278337

[4] Lee H, Chung W (2018) Terrain Classification for Mobile Robots on the Basis of Support Vector Data Description. International Journal of Precision Engineering and Manufacturing 19(9):1305–1315, DOI 10.1007/s12541-018-0154-4

[5] Noguchi H, Handa M, Fukui R, Mori T, Sato T, Sanada H (2012) Capturing Device for Dense Point Cloud of Indoor People using Horizontal LIDAR and Pan Rotation of Vertical LIDAR with Mirrors. In: IEEE/SICE International Symposium on System Integration (SII), pp 428–433

[6] Ohno K, Tadokoro S, Nagatani K, Koyanagi E, Yoshida T (2010) Trials of 3-D map construction using the tele-operated tracked vehicle kenaf at disaster city. In: 2010 IEEE International Conference on Robotics and Automation, pp 2864–2870, DOI 10.1109/ROBOT.2010.5509722

[7] Quigley M, Conley K, Gerkey B, Faust J, Foote T, Leibs J, Wheeler R, Ng AY (2009) Ros: an open-source robot operating system. In: ICRA workshop on open source software, Kobe, Japan, vol 3, p 5

[8] Sinha A, Papadakis P (2013) Mind the gap: detection and traversability analysis of terrain gaps using LIDAR for safe robot navigation. Robotica 31:1085–1101, DOI 10.1017/S0263574713000349

[9] Transport Ministry of Land I, (MLIT) T (2014) Efforts to take a far-sighted vision of social infrastructures. URL `http://www.mlit.go.jp/common/001063080.pdf`

[10] Westfechtel T, Ohno K, Mertsching B, Hamada R, Nickchen D, Kojima S, Tadokoro S (2018) Robust stairway-detection and localization method for mobile robots using a graph-based model and competing initializations. International Journal of Robotics Research 37(12):1463–1483, DOI 10.1177/0278364918798039